Effects of Anthropogenic Forcings on Multidecadal Variability of the Sea Level around the Japanese Coast Simulated by MRI-ESM2.0 for CMIP6

Yusuke Ushijima[1], Hiroyuki Tsujino[2], Kei Sakamoto[2], Masayoshi Ishii[3], Tsuyoshi Koshiro[2], and Naga Oshima[2]

[1]Japan Meteorological Business Support Center
[2]Meteorological Research Institute
[3]Meteorological Research Institute, Japan

November 26, 2022

Abstract

The observed sea level (SL) around the Japanese coast shows a peculiar multidecadal variation with the peak in the 1950s followed by the gradual fall until the 1970s and the rebound continuing to the present, making the recent SL rise less remarkable in the historical record. An ensemble mean of the historical simulations conducted for the Coupled Model Intercomparison Project phase 6 (CMIP6) using the Meteorological Research Institute Earth System Model version 2.0 (MRI-ESM2.0) reproduces this variability well, implying that this was a forced one. The MRI-ESM2.0 simulations for the Detection and Attribution Model Intercomparison Project suggest that the increase in anthropogenic aerosols caused the SL fall from the 1950s to the 1970s and the increase in greenhouse gases caused the SL rise after that. Additional sensitivity runs indicate that the surface heat loss in the North Pacific due to anthropogenic aerosols plays a dominant role in the SL fall.

Effects of Anthropogenic Forcings on Multidecadal Variability of the Sea Level around the Japanese Coast Simulated by MRI-ESM2.0 for CMIP6

Yusuke Ushijima[1,2], Hiroyuki Tsujino[2], Kei Sakamoto[2], Masayoshi Ishii[2], Tsuyoshi Koshiro[2], Naga Oshima[2]

[1]Japan Meteorological Business Support Center, Tsukuba, Japan

[2]Meteorological Research Institute, Tsukuba, Japan

Key Points:

- The Meteorological Research Institute Earth System Model version 2.0 reproduces the multidecadal sea level variation around Japan since 1950
- The sea level fall around Japan from the 1950s to the 1970s is likely due to the increase in anthropogenic aerosols
- Surface heat loss in the North Pacific due to anthropogenic aerosols plays a dominant role in the sea level fall

Corresponding author: Yusuke Ushijima, usijimay@mri-jma.go.jp

Abstract

The observed sea level (SL) around the Japanese coast shows a peculiar multidecadal variation with the peak in the 1950s followed by the gradual fall until the 1970s and the rebound continuing to the present, making the recent SL rise less remarkable in the historical record. An ensemble mean of the historical simulations conducted for the Coupled Model Intercomparison Project phase 6 (CMIP6) using the Meteorological Research Institute Earth System Model version 2.0 (MRI-ESM2.0) reproduces this variability well, implying that this was a forced one. The MRI-ESM2.0 simulations for the Detection and Attribution Model Intercomparison Project suggest that the increase in anthropogenic aerosols caused the SL fall from the 1950s to the 1970s and the increase in greenhouse gases caused the SL rise after that. Additional sensitivity runs indicate that the surface heat loss in the North Pacific due to anthropogenic aerosols plays a dominant role in the SL fall.

Plain Language Summary

The coastal sea level change is important because it significantly affects human activity. It is known that the sea level around Japan fell from the 1950s to the 1970s and rose from the 1980s. However, the reason for this long-term sea level change around Japan has not been well understood. In this study, the sea level around Japan in a suite of simulations by a climate model, the Meteorological Research Institute Earth System Model version 2.0, is analyzed and the cause of the sea level change is investigated. In the historical simulations of the climate model, both the sea level fall from the 1950s to the 1970s and the sea level rise from the 1980s occur around Japan. From the analysis of the sensitivity simulations to separately evaluate effects of anthropogenic forcings, it is suggested that the increase in anthropogenic aerosols caused the sea level fall and that in greenhouse gases caused the sea level rise. Especially, surface heat loss in the North Pacific due to anthropogenic aerosols is likely to have a dominant role in the sea level fall.

1 Introduction

The sea level (SL) variability in the coastal region is important because it affects the natural environment and socio-economic activities. Although the global mean SL is persistently rising (e.g., Church & White, 2011), the recent SL rise around the Japanese coast catches less attention. This is because the multidecadal variability of the SL, with

the fall from the 1950s to the 1970s and the rise from the 1980s, is more remarkable (e.g., Sasaki et al., 2017) (see also Fig. 1a).

This SL multidecadal variability with a 50–60 year period has been considered as part of natural variabilities because it was not reproduced by the multi-model ensemble mean of the historical simulations by the Coupled Model Intercomparison Project (CMIP) phase 5 (CMIP5) models (Sasaki et al., 2017). However, the historical simulations of our new earth system model [the Meteorological Research Institute Earth System Model version 2.0 (MRI-ESM2.0)] (Yukimoto et al., 2019) developed for CMIP phase 6 (CMIP6) appear to reproduce the observed multidecadal SL variability around the Japanese coast after the middle of the 20th century (Fig. 1a) when the anthropogenic climate forcers such as greenhouse gasses and aerosols started to take nontrivial effects. This suggests a possibility that the anthropogenic forcings have caused the multidecadal variability.

Among the anthropogenic forcings, the greenhouse gasses are well known to raise the global mean thermosteric SL (TSL) by increasing the global ocean heat uptake. It is also projected that the increase in greenhouse gases eventually causes the change in the SL spatial distribution. Specifically, the dynamic SL (DSL) rises in the western subtropical North Pacific owing to the subtropical mode water (STMW) warming in the recent decades (Suzuki & Ishii, 2011, 2015) and in the future (Terada & Minobe, 2018; Suzuki & Tatebe, 2020).

On the other hand, anthropogenic aerosols in the atmosphere could cause the "global dimming", the decrease in the downward shortwave radiation at the surface, from the 1950s to the 1980s (Liepert, 2002; Wild, 2016). This dimming differs vastly between regions (Wild et al., 2007); the strong dimming in East Asia could have been affecting the climate state in the North Pacific (Boo et al., 2015) including the SL around the Japanese coast before greenhouse gases start to dominate anthropogenic climate change (e.g., Jones et al., 2013). However, the effects of the dimming on the SL have not been properly incorporated or evaluated in previous simulations by ocean-only models or CMIP multimodels because of the lack of temporal variation of aerosols in most reanalysis data (Fujiwara et al., 2017) used for calculating surface fluxes in ocean-only models or the difficulty in reproducing the response to the aerosols in climate models (Storelvmo et al., 2018; Moseid et al., 2020), which might cause the multidecadal SL variation indiscernible in CMIP5 models. Although most CMIP6 models largely underestimated the observed dimming

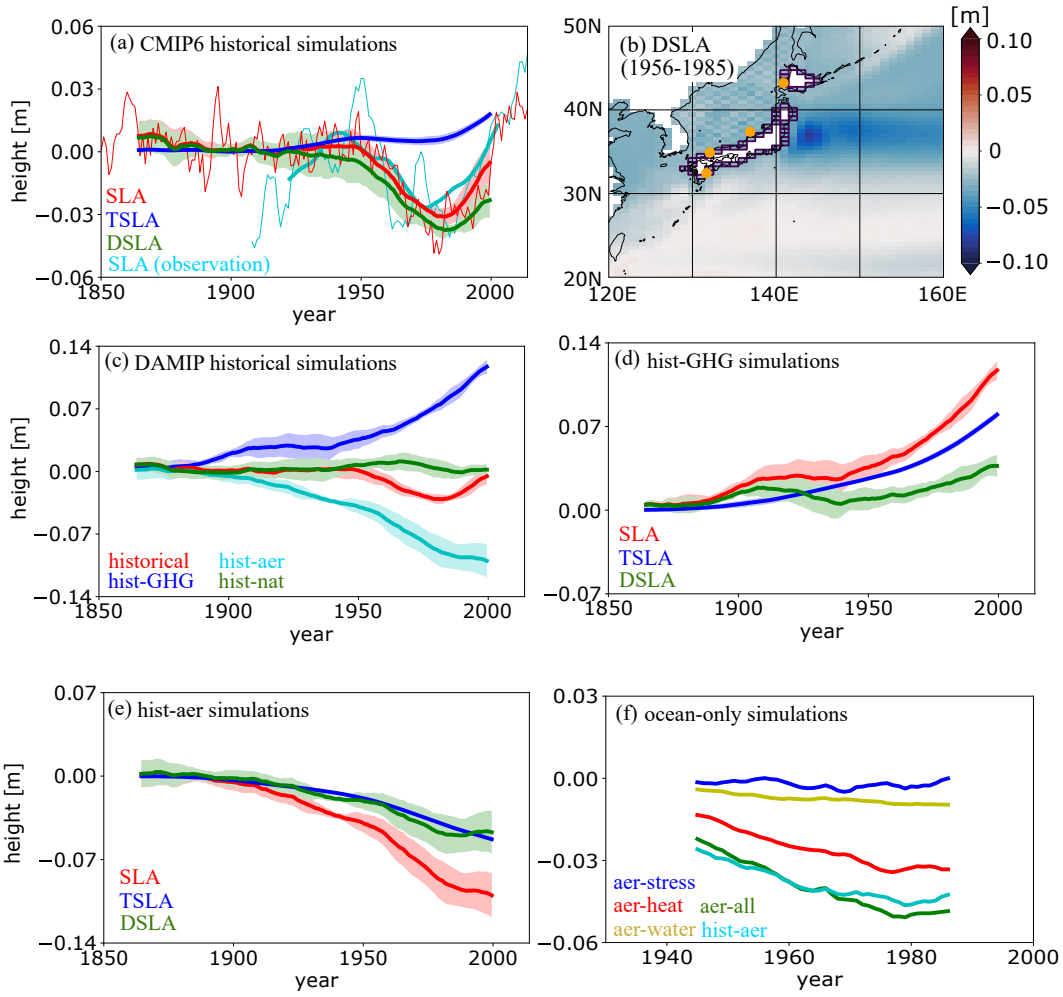

Figure 1. (a) Time series of the ensemble mean SL anomaly (SLA) (red), thermosteric SL anomaly (TSLA) (blue), and dynamic SL anomaly (DSLA) (green) around the Japanese coast in the historical simulations and the observed SLA (cyan). (b) The ensemble mean DSLA in the historical simulations averaged in 1956–1985. Time series of (c) the ensemble mean SLA in the historical (red), hist-GHG (blue), hist-aer (cyan), and hist-nat (green) simulations. Time series of the ensemble mean SLA (red), TSLA (blue), and DSLA (green) around the Japanese coast in the (d) hist-GHG and (e) hist-aer simulations. (f) Time series of the DSLA around the Japanese coast in the ocean-only-aer-stress (blue), ocean-only-aer-heat (red), ocean-only-aer-water (yellow), ocean-only-aer-all (green), and hist-aer (cyan) simulations. Thin lines in (a) are annual mean values, and thick lines are 30-year running mean values. Shades in (a) and (c)-(e) represent the spread of the simulations (±1 standard deviation). The orange circles and purple rectangles in (b) represent the tide gauge stations and the grids used to calculate the DSLA around the Japanese coast, respectively.

over East Asia, MRI-ESM2.0 showed the evolution of the dimming most similar to the observations (Moseid et al., 2020), which enables a reliable estimate of effects of anthropogenic aerosols on the SL around the Japanese coast. It would be of particular interest to seek the possibility that the increase in anthropogenic aerosols reduced the surface heat uptake in the North Pacific and also the SL around the Japanese coast from the 1950s to the 1970s (or the 1980s) in MRI-ESM2.0. Note that our historical simulations fail to reproduce the SL variability before the middle of the 20th century when natural variabilities would have dominated effects of anthropogenic forcings. So, we will focus on the effect of the anthropogenic forcing on the SL around Japan after the middle of the 20th century using MRI-ESM2.0 in this study.

To reveal the processes how anthropogenic forcings cause the SL change, we made use of process-oriented model intercomparison projects (MIPs) endorsed by CMIP6. Detection and Attribution MIP (DAMIP) (Gillett et al., 2016) is used to quantify the effects of each anthropogenic or natural forcing. To compare the relative contributions from surface heat, momentum, and fresh water flux anomalies caused by anthropogenic aerosols to the SL change around Japan, sensitivity experiments using a framework similar to the Flux-Anomaly-Forced MIP (FAFMIP) (Gregory et al., 2016) are also conducted.

This paper is organized as follows. In section 2, the data used in this study and the configurations of the sensitivity experiments are described. Then, the SL around the Japanese coast in the CMIP6 historical simulations by MRI-ESM2.0 is compared to the observed SL in section 3. From the results of the experiments conducted for DAMIP using MRI-ESM2.0, the effects of the anthropogenic forcings on the multidecadal variability of the SL around the Japanese coast are investigated. Results of the FAFMIP-like sensitivity experiments are used to discuss what surface flux anomalies due to the anthropogenic aerosol forcings are most responsible for the simulated changes. In section 4, the conclusion of this study is described.

2 Method

2.1 Data

The simulations by MRI-ESM2.0 (Yukimoto et al., 2019; Kawai et al., 2019; Oshima et al., 2020) conducted for CMIP6 are used to investigate the temporal variation of the SL around the Japanese coast. An ensemble of 5 members of the CMIP6 histor-

ical simulations (1850–2014) starting from different initial conditions taken from the piControl simulation on January 1st in 1850, 1900, 1950, 2000, and 2050 is compared to the observed data, examining whether the multidecadal variability of the SL after the middle of the 20th century is reproduced. The observed data is a simple average of the SL at four tide gauge stations around Japan (circles in Fig. 1b), which can be obtained from the Japan Meteorological Agency (JMA) website (`http://www.data.jma.go.jp/gmd/kaiyou/english/sl_trend/sea_level_around_japan.html`).

To examine whether any external forcing is driving the multidecadal variability of the SL around Japan in the historical simulations or not, the results of a series of experiments conducted for DAMIP (Gillett et al., 2016) using MRI-ESM2.0 are analyzed. We used three types of the DAMIP simulations, well mixed greenhouse-gas-only historical (hist-GHG), anthropogenic-aerosol-only historical (hist-aer), and natural solar irradiance forcing- and volcanic forcing-only historical (hist-nat) simulations with each simulation consisting of 5 ensemble members starting from corresponding initial conditions in the historical simulations. The list of experiments by MRI-ESM2.0 is summarized in Table S1.

The SL around the Japanese coast from model outputs is calculated by the sum of the global mean TSL (the CMIP6 output variable "zostoga") and the DSL (the CMIP6 output variable "zos") averaged around the Japanese coast, consisting of the grid points next to land grid points representing Japanese Islands in MRI-ESM2.0 (purple rectangles in Fig 1b). Since the DSL averaged for 30 years is almost uniform around the Japanese coast probably due to the coastal trapped waves as shown in Fig 1b and the DSL averaged around the Japanese coast has almost the same value as the DSL averaged at the four grid points closest to the four tide gauge stations in the historical simulations (not shown), we compared the SL averaged around the Japanese coast with the observed SL averaged in the four tide gauge stations. Note that the global SL changes due to the halosteric contraction/expansion and water mass change are ignored in this study. In comparison to the TSL change, the halosteric SL change is too small and thus has been omitted from the Ocean MIP output variables (Griffies et al., 2016). In MRI-ESM2.0, the melting of glaciers and ice sheets is not fully considered, and hence the global water mass in the ocean hardly changes. It is suggested that the SL change due to the water mass change was comparable to the TSL change (Mitrovica et al., 2006; Chen et al., 2017) and became small from the 1950s to the 1970s (Slangen et al., 2017). This indicates that the

SL change due to water mass change is expected to be much smaller than the DSL change from the 1950s to the 1970s and to have a minor impact on our conclusions qualitatively, though it might explain the underestimation of the recent SL in the MRI-ESM2.0 historical simulation (Fig. 1a).

2.2 Analysis

To consider multidecadal variability with a 50–60 year period, a 30-year running mean is applied to the SL, TSL, and DSL. The ensemble mean of deviations of the historical simulations (including the DAMIP simulations) relative to the piControl simulation at the same elapsed time since the branching off are analyzed. The observed SL anomaly (SLA) relative to its average of 1937–1966, when the SLA in the historical simulations relative to the piControl simulation is almost zero, is used to evaluate the simulated SLA.

We additionally compare the effects of the surface flux changes due to anthropogenic aerosols on the SL change through sensitivity experiments using a framework similar to FAFMIP (Gregory et al., 2016). To quantify the relative contribution of each surface flux, the surface flux changes are added to the fluxes without anthropogenic aerosols, and ocean-only simulations are performed with the fluxes. The surface flux changes are the time series of the monthly mean anomaly in a member of the hist-aer simulations relative to the piControl simulation that was run in parallel (i.e., that shared the initial condition). The fluxes without anthropogenic aerosols are calculated in the ocean model using the 3-hourly atmospheric data of the piControl simulation and the simulated surface ocean state of the ocean-only simulation. We used a hist-aer simulation that started in 1850 of the piControl simulation, which shows the SLA similar to the ensemble mean. The surface wind stress anomaly (ocean-only-aer-stress), the surface heat flux anomaly (ocean-only-aer-heat), the surface water flux anomaly (ocean-only-aer-water), and the wind stress, surface heat flux, and surface water flux anomalies (ocean-only-aer-all) are added separately to the fluxes without anthropogenic aerosols in the sensitivity simulations. An ocean-only control simulation, corresponding to the piControl simulation, was also performed without any flux anomaly. (The details for the flux calculation are described in Text S1, and the list of sensitivity experiments is summarized in Table S2.) For the ocean model, the MRI community ocean model version 4 (MRI-COM4) (Urakawa et al., 2020), which is the ocean component of MRI-ESM2, is used. From the piControl output on Jan-

uary 1st in 1930, 5 simulations that differ in surface forcing as described above are started and continued for 71 years. Note that the anomalies of the 30-year running mean variables relative to the control simulation are analyzed as in the historical and DAMIP simulations.

3 Results

3.1 Effects of Anthropogenic Forcings on the SL around the Japanese Coast in the Historical Simulations of MRI-ESM2.0

Figure 1a illustrates the time series of the ensemble mean SLA around the Japanese coast in the historical simulations relative to the piControl simulation and the observed SLA. The 30-year running mean SLA in the historical simulations followed that of the observed data well; the SL fell from the 1950s to the 1970s and rose after the 1980s. On the other hand, the observed SLA in the decadal and interdecadal ($\sim$ 10–20 years period) time scales (e.g., the rapid fall and rise in the 1950s and the early 1970s, respectively), which is generally considered to be governed by natural variability, are not reproduced although their amplitudes are comparable to the multidecadal ones. Considering that the anthropogenic forcings take non-negligible effects after around the 1950s, the observed multidecadal variability of the SL might have been caused by the anthropogenic forcings. Note that the SLA seen in the historical simulations by MRI-ESM2.0 are followed by the DSL anomaly (DSLA) better than the TSL anomaly, especially from the 1950s to the 1970s (Fig.1a), and also that the fall of the DSL around the Japanese coast is accompanied by that in the western North Pacific (Fig. 1b). These results suggest that the SL change around the Japanese coast can be represented by that of the western North Pacific as described in previous studies (Yasuda & Sakurai, 2006; Sasaki et al., 2017).

To investigate the effects of the anthropogenic forcings on the multidecadal variability of the SL around the Japanese coast in MRI-ESM2.0, the result of the DAMIP experiments by MRI-ESM2.0 is used. Figure 1c shows the time series of the 30-year running mean SLAs in the historical, hist-GHG, hist-aer, and hist-nat simulations. The change in the ensemble mean of the hist-nat simulations is smaller than those in the hist-GHG and hist-aer simulations. In the hist-GHG simulations, the SL keeps rising and its trend gets stronger after the middle of the 20th century, which explains the SL rise after the

1980s in the historical simulations by MRI-ESM2.0. The TSLA is larger than DSLA (Fig. 1d) in hist-GHG. On the other hand, the SLA in the hist-aer simulations falls with time, especially from the 1950s to the 1970s (Fig. 1c). In the hist-aer simulations, the DSLA is comparable to the TSLA, and it shows the considerable decline from the 1950s to the 1970s (Fig. 1e). Thus, the temporal variation of the DSLA due to anthropogenic aerosols is an important factor to explain the SL fall around the Japanese coast seen in the MRI-ESM2.0 historical simulations.

Anthropogenic aerosols affect the surface heat flux since net shortwave radiation (SWR) is inhibited by aerosol radiation interaction (ARI) and aerosol cloud interaction (ACI). In the hist-aer simulations, the surface heat flux anomaly relative to the piControl simulation averaged in 1956–1985 is negative, that is, the heat is lost from the ocean to the atmosphere in the western North Pacific (Fig. 2a) mainly due to the SWR reduction (~ -10 W m^{-2}) (Figs. 2b-d) except for the latitudinal band around 40°N (Fig. 2a) where surface turbulent heat fluxes cause the heat uptake (Fig. 2d). The negative SWR anomaly in the hist-aer simulations well corresponds to the positive anomaly of aerosol optical depth (Fig. 2e) and negative anomaly of SWR difference between all sky and clear sky (Fig. 2f), implying the ARI and ACI effects cause the heat loss in the western North Pacific. Due to this net surface heat loss in the ocean, the sea surface temperature (SST) decreases by ~ 1 °C (Fig. 2g), and its horizontal distribution shows a PDO-like pattern (Zhong & Liu, 2009; Zhang & Delworth, 2015). Probably related to this SST anomaly pattern, Aleutian low is intensified (Fig. 2h) like PDO. Since intensified Aleutian low can cause the fall of the SL around Japan (Sasaki et al., 2017), we used a 1.5 layer reduced gravity model (Eq. 2 of Qiu, 2003), whose DSLA is generated by wind stress curl anomaly and is propagated by the first-mode baroclinic Rossby wave, and evaluated its impacts on the DSLA in the North Pacific. As a result, this simple DSLA evaluation using the 1.5 layer model (Fig 2i) does not explain the DSLA pattern simulated in MRI-ESM2.0 (Fig 2j). This implies that the DSL change is not explained by wind stress change alone and surface heat flux change would be also an important factor causing the DSL fall.

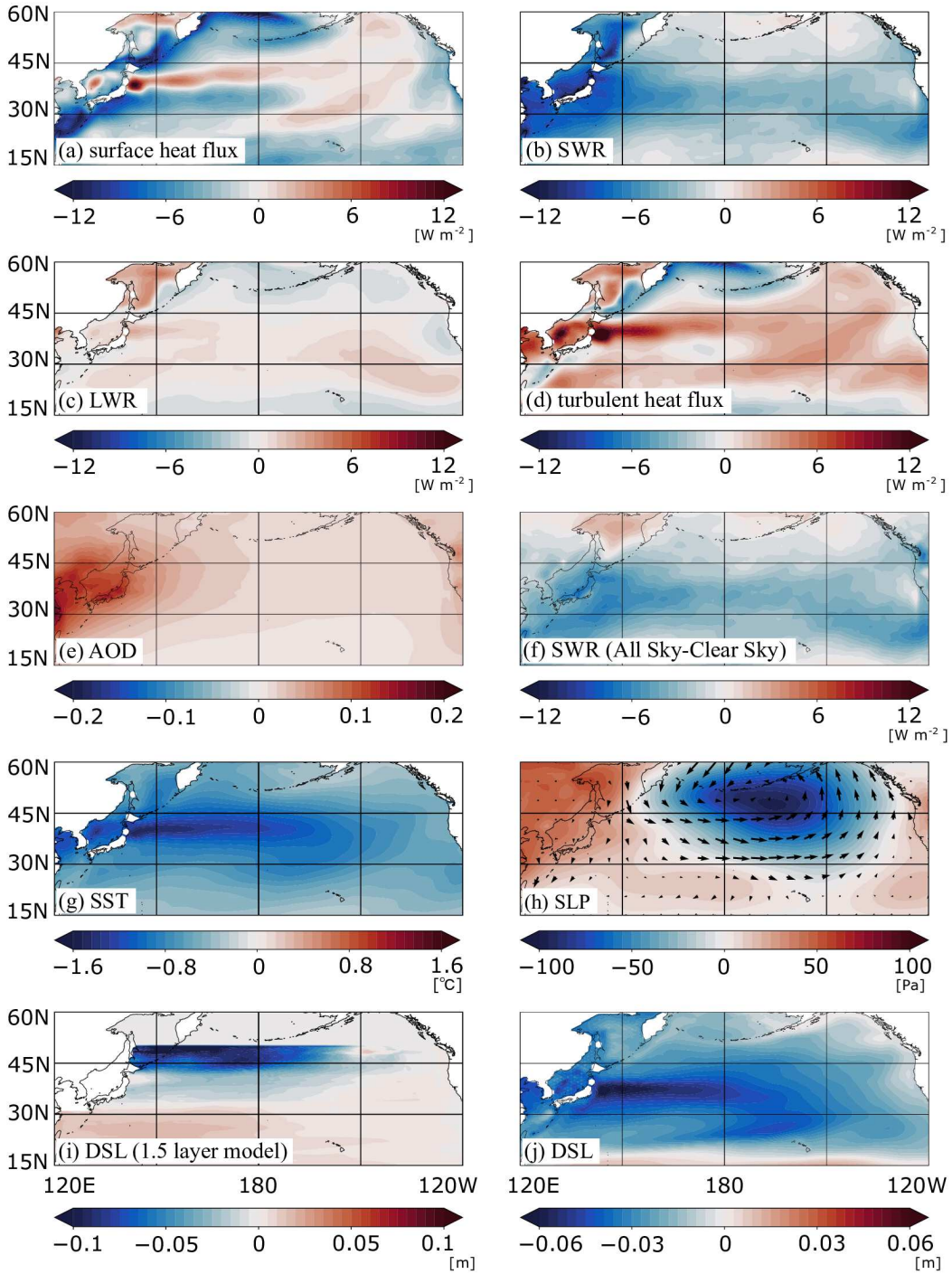

Figure 2. The ensemble mean anomalies of the (a) net surface heat flux, (b) SWR, (c) net longwave radiation (LWR), (d) net surface turbulent (sensible plus latent) heat flux, (e) aerosol optical depth (AOD) at 550 nm, (f) SWR difference between all sky and clear sky, (g) SST, (h) sea level pressure with wind stress anomaly (vector), (i) DSL evaluated by using 1.5 layer model, and (j) simulated DSL in the North Pacific in the hist-aer simulations relative to the piControl simulation averaged in 1956–1985.

3.2 Effects of the Surface Flux Changes due to Anthropogenic Aerosols on the SL around the Japanese Coast

To evaluate the relative contribution to the DSL fall around the Japanese coast from the changes of the wind stress, surface heat flux, and surface water flux, we conducted additional sensitivity experiments where the changes of these fluxes are imposed separately. Figure 1f shows the temporal variation of the DSLA around the Japanese coast in the ocean-only-aer-stress, ocean-only-aer-heat, ocean-only-aer-water, and ocean-only-aer-all simulations as well as the member of the hist-aer simulations from which the flux anomalies are taken. The 30-year running mean DSLA in the ocean-only-aer-all simulation falls until 1980 and is almost coincident with that in the hist-aer simulation, indicating that the surface flux changes in these simulations explain the DSLA in the hist-aer simulation. The DSL change in the ocean-only-aer-heat simulation is larger than those in the ocean-only-aer-stress and ocean-only-aer-water simulations. The 30-year running mean DSLA in 1980 in the ocean-only-aer-stress, ocean-only-aer-heat, ocean-only-aer-water, and ocean-only-aer-all simulations are -3.36×10^{-3} m, -3.30×10^{-2} m, -9.50×10^{-3} m, and -5.03×10^{-2} m, respectively, that is, wind stress, surface heat flux, and surface water flux changes explain the DSL change due to all flux change by 6.67 %, 65.5 %, and 18.9 %, respectively. Thus, the contribution from the surface heat flux change due to anthropogenic aerosols to the DSL is larger than those from the other fluxes. Note that the remaining $\sim$ 9 % difference between the ocean-only-aer-all DSLA and the sum of the ocean-only-aer-stress, ocean-only-aer-heat, and ocean-only-aer-water DSLAs would be explained by non-linear effects as discussed later.

Despite the intensified Aleutian low is suggested to reduce the DSL around Japan (Sasaki et al., 2017), the wind stress change has a little effect on the DSL for this case. To consider this reason, the DSLA in the North Pacific averaged in 1956–1985 are shown in Figs. 3a-d. In the ocean-only-aer-stress simulation, the DSLA is actually negative in the subarctic North Pacific (Fig. 3a) due to the intensified Aleutian low (Fig. 2h) but becomes positive in the subtropical North Pacific (Fig. 3a) due to the positive pressure (negative wind stress curl) anomaly (Fig. 2h) as in Fig. 2i, indicating this response is caused by baroclinic Rossby waves. As a result, the positive and negative DSLAs cancel each other out, when they are integrated along the eastern coast of Japan for estimating an average SL change around Japan (e.g., Tsujino et al., 2008; Minobe et al.,

2017). Thus, the wind stress change hardly affects the DSL around Japan (Fig. 1f) though it redistributes the DSL in the North Pacific (Fig. 3a).

In the ocean-only-aer-heat simulation, on the other hand, the DSL falls in the whole North Pacific and the DSL fall is the largest in the western subtropical North Pacific (Fig. 3b). To see how surface heat flux changes the DSL in the western North Pacific, the latitude-depth sections of the dynamic height and temperature anomalies averaged in 1956–1985 at 150° E are shown in Figs. 3e-l. Here, the dynamic height anomaly is calculated as

$$\frac{1}{g}\int_{p_B}^{p}\left(\frac{1}{\rho}-\frac{1}{\rho_c}\right)dp' \cong \rho_0\int_{H}^{z}\left(\frac{1}{\rho}-\frac{1}{\rho_c}\right)dz' = \text{dynamic height anomaly}, \qquad (1)$$

where ρ is the density, ρ_c is the density in the control simulation, $\rho_0 (= 1.036\times10^3$ kg m$^{-3})$ is the reference density, p (p') is the pressure, p_B is the bottom pressure, g is the acceleration due to gravity, z (z') is the ocean depth, and H is the depth of the ocean floor. The dynamic height anomaly in the ocean-only-aer-heat simulation shows the particular change in the south of 40° N at 150° E and is confined in the upper ocean ($<$ 400 m) (Fig. 3f). This change is explained by the temperature decrease in the Kuroshio Extension (KE) region ($35° - 40°$ N) above 1000 m and in the south of 35° N above 400 m (Fig. 3j), corresponding to the STMW although DSL change due to cooling is relatively small in the north of 40° N above 1000 m because of the compensating low salinity anomaly. Thus, the DSL in the western North Pacific falls due to the colder (denser) KE and STMW in the ocean-only-aer-heat simulation. Since the linear combination of the variables in the ocean-only-aer-stress, ocean-only-aer-heat, and ocean-only-aer-water simulations explains most of those in the ocean-only-aer-all simulation (Fig. 3) and the contribution of the surface heat flux to the DSLA is larger than those of the other flux changes (Fig. 1f), it is indicated that the colder KE and STMW by surface heat flux change due to the increase in anthropogenic aerosols lower the DSL in the western North Pacific and hence around Japan.

Note that observed data shows that the STMW causes the multidecadal variation of the DSL in the western North Pacific and lowers the DSL in the 1970s and 1980s, consistent with our results, while the first-mode baroclinic Rossby waves cause the interdecadal variations (Suzuki & Ishii, 2015). This implies that the surface flux change has an impact on the multidecadal variation of the DSL in the western North Pacific as described above while wind stress change causes the decadal and interdecadal variation as suggested by Sasaki et al. (2017). Furthermore, the surface heat flux and wind stress changes

nonlinearly interact with each other. Regarding the part of the SL fall in the ocean-only-aer-all simulation unexplained by the simple sum of the sensitivity simulations, it is concentrated in the region south and east of Japan (Figs. 3c and d). This is probably because the more cooled water in the western part of the subtropical gyre as seen in the ocean-only-aer-heat simulation (Fig. 3b) is transported to the region southeast of Japan by the intensified subtropical gyre due to wind stress anomaly in the ocean-only-aer-stress simulation (Fig. 3a), which could be regarded as a non-linear effect.

4 Conclusion

In this study, the SL variability around the Japanese coast in the CMIP6 historical simulations by MRI-ESM2.0 was investigated. MRI-ESM2.0 reproduces the observed multidecadal variability of the SL around the Japanese coast; the SL fell from the 1950s to the 1970s and rose from the 1980s. To evaluate the effects of the anthropogenic forcings on the multidecadal SL variability, the results of the DAMIP historical simulation by MRI-ESM2.0 were analyzed. It was found that the increase in anthropogenic aerosols eventually causes the SL fall from the 1950s to the 1970s while greenhouse gas forcing raises the SL after the 1980s. The surface heat loss to the atmosphere from the North Pacific increases and the Aleutian low is intensified in 1956–1985 due to anthropogenic aerosols in the MRI-ESM2.0 simulations, which can lower the SL around Japan. Sensitivity experiments similar to the FAFMIP experiments were conducted to compare the effects of the surface heat flux and wind stress change due to anthropogenic aerosols. The surface heat flux change has a dominant role in the SL fall around Japan through the cooling of the KE and STMW, while the impact of the wind stress change on the DSL change around Japan was minor in the present case. These results provide the possibility that the multidecadal variability of the SL around the Japanese coast in the latter half of the 20th century was caused by the anthropogenic forcings.

Note that the responses to anthropogenic aerosols vary significantly among the CMIP6 models although MRI-ESM2.0 is among the most successful models in reproducing the observed shortwave radiation change in East Asia (Moseid et al., 2020). This large uncertainty makes it difficult to quantify the effects of the anthropogenic forcings on the DSL in the North Pacific and around Japan and to compare them with those of natural variability using a multi-model approach. For more precise assessments, further improvement of the climate models is needed.

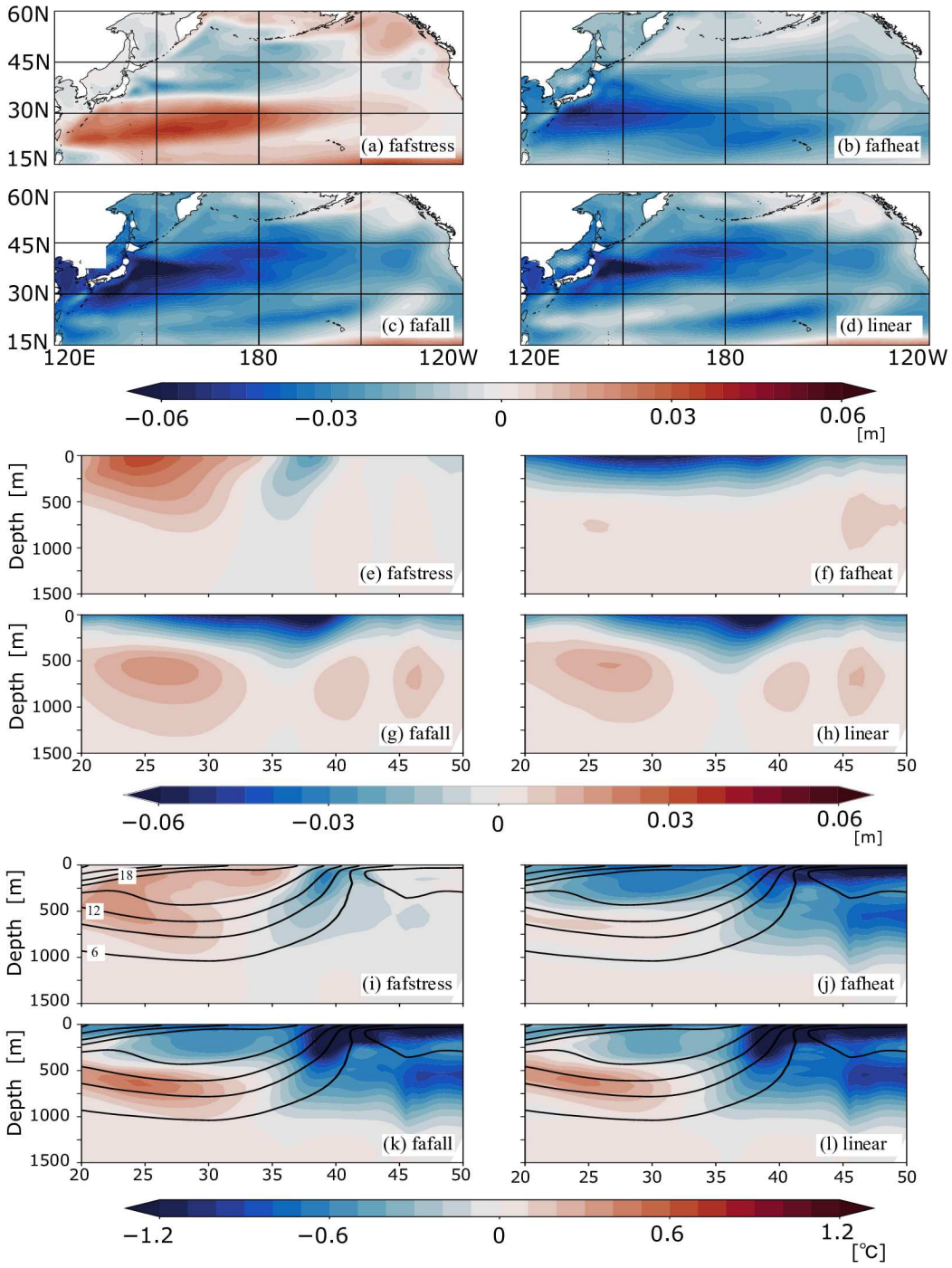

Figure 3. (a)-(d) The DSLA in the North Pacific and latitude-depth sections of the (e)-(h) dynamic height and (i)-(l) temperature anomalies in the (a), (e), (i) ocean-only-aer-stress, (b), (f), (j) ocean-only-aer-heat, and (c), (g), (k) ocean-only-aer-all simulations. The panel (d), (h), and (l) are the linear combinations of the variables in the ocean-only-aer-stress, ocean-only-aer-heat, and ocean-only-aer-water simulations. All variables are averaged in 1956–1985. Lines in (i)-(l) represent the temperature in the control simulation.

Open Research

Data Availavility Statement

The data of MRI-ESM2.0 for CMIP6 can be accessed from the website of ESGF (`https://esgf-node.llnl.gov/`). The variant labels of r1i1p1f1, r2i1p1f1, r3i1p1f1, r4i1p1f1, and r5i1p1f1 in the historical, hist-GHG, hist-aer, and hist-nat simulations and r1i1p1f1 in the piControl simulations were used in this study. The observed SL data at the four stations around the Japanese coast was obtained from the JMA website (`http://www.data.jma.go.jp/gmd/kaiyou/english/sl_trend/sea_level_around_japan.html`). The sensitivity experiment data are available at `https://climate.mri-jma.go.jp/pub/archives/Ushijima-et-al_SL`.

Acknowledgments

This work was supported by the Integrated Research Program for Advancing Climate Models (TOUGOU) Grant Number JPMXD0717935561 and MEXT-Program for the advanced studies of climate change projection (SENTAN) Grant Number JPMXD0722680734 from the Ministry of Education, Culture, Sports, Science and Technology (MEXT), Japan and the Environment Research and Technology Development Fund (JPMEERF20202003 and JPMEERF20205001) of the Environmental Restoration and Conservation Agency of Japan.

References

Boo, K.-O., Booth, B. B. B., Byun, Y.-H., Lee, J., Cho, C., Shim, S., & Kim, K.-T. (2015). Influence of aerosols in multidecadal SST variability simulations over the North Pacific. *J. Geophys. Res.-Atmos.*, *120*(2), 517–531. doi: 10.1002/2014JD021933

Chen, X., Zhang, X., Church, J. A., Watson, C. S., King, M. A., Monselesan, D., ... Harig, C. (2017). The increasing rate of global mean sea-level rise during 1993–2014. *Nature Clim. Change*, *7*(7), 492–495. doi: 10.1038/nclimate3325

Church, J. A., & White, N. J. (2011). Sea-Level Rise from the Late 19th to the Early 21st Century. *Surv. Geophys.*, *32*(4-5), 585–602. doi: 10.1007/s10712-011-9119-1

Fujiwara, M., Wright, J. S., Manney, G. L., Gray, L. J., Anstey, J., Birner, T., ...

359 others (2017). Introduction to the sparc reanalysis intercomparison project
360 (s-rip) and overview of the reanalysis systems. *Atmos. Chem. Phys.*, *17*(2),
361 1417–1452. doi: 10.5194/acp-17-1417-2017

362 Gillett, N. P., Shiogama, H., Funke, B., Hegerl, G., Knutti, R., Matthes, K., ...
363 Tebaldi, C. (2016). The Detection and Attribution Model Intercomparison
364 Project (DAMIP v1.0) contribution to CMIP6. *Geosci. Model Dev.*, *9*(10),
365 3685–3697. doi: 10.5194/gmd-9-3685-2016

366 Gregory, J. M., Bouttes, N., Griffies, S. M., Haak, H., Hurlin, W. J., Jungclaus,
367 J., ... Winton, M. (2016). The Flux-Anomaly-Forced Model Intercompari-
368 son Project (FAFMIP) contribution to CMIP6: Investigation of sea-level and
369 ocean climate change in response to CO2 forcing. *Geosci. Model Dev.*, *9*(11),
370 3993–4017. doi: 10.5194/gmd-9-3993-2016

371 Griffies, S. M., Danabasoglu, G., Durack, P. J., Adcroft, A. J., Balaji, V., Böning,
372 C. W., ... others (2016). Omip contribution to cmip6: Experimental and diag-
373 nostic protocol for the physical component of the ocean model intercomparison
374 project. *Geosci. Model Dev.*, *9*(9), 3231–3296. doi: 10.5194/gmd-9-3231-2016

375 Jones, G. S., Stott, P. A., & Christidis, N. (2013). Attribution of observed histor-
376 ical near–surface temperature variations to anthropogenic and natural causes
377 using cmip5 simulations. *J. Geophys. Res.-Atmos.*, *118*(10), 4001–4024. doi:
378 10.1002/jgrd.50239

379 Kawai, H., Yukimoto, S., Koshiro, T., Oshima, N., Tanaka, T., Yoshimura, H., &
380 Nagasawa, R. (2019). Significant improvement of cloud representation in
381 global climate model MRI-ESM2. *Geosci. Model Dev.*, *2*(7), 2875–2897. doi:
382 10.5194/gmd-12-2875-2019

383 Liepert, B. G. (2002). Observed reductions of surface solar radiation at sites in the
384 United States and worldwide from 1961 to 1990. *Geophys. Res. Lett.*, *29*(10),
385 61–1–61–4. doi: 10.1029/2002gl014910

386 Minobe, S., Terada, M., Qiu, B., & Schneider, N. (2017). Western boundary sea
387 level: a theory, rule of thumb, and application to climate models. *J. Phys.*
388 *Oceanogr.*, *47*(5), 957–977. doi: 10.1175/JPO-D-16-0144.1

389 Mitrovica, J. X., Wahr, J., Matsuyama, I., Paulson, A., & Tamisiea, M. E. (2006).
390 Reanalysis of ancient eclipse, astronomic and geodetic data: A possible route
391 to resolving the enigma of global sea-level rise. *Earth Planet. Sci. Lett.*, *243*(3-

4), 390–399. doi: 10.1016/j.epsl.2005.12.029

Moseid, O. K., Schulz, M., Storelvmo, T., Rian Julsrud, I., Olivié, D., Nabat, P., ... Gastineau, G. (2020). Bias in CMIP6 models as compared to observed regional dimming and brightening. *Atmos. Chem. Phys.*, *20*(24), 16023–16040. doi: 10.5194/acp-20-16023-2020

Oshima, N., Yukimoto, S., Deushi, M., Koshiro, T., Kawai, H., Tanaka, T. Y., & Yoshida, K. (2020). Global and Arctic effective radiative forcing of anthropogenic gases and aerosols in MRI-ESM2.0. *Prog. Earth Planet. Sci.*, *7*(1), 1–21. doi: 10.1186/s40645-020-00348-w

Qiu, B. (2003). Kuroshio extension variability and forcing of the Pacific decadal oscillations: Responses and potential feedback. *J. Phys. Oceanogr.*, *33*(12), 2465–2482. doi: 10.1175/2459.1

Sasaki, Y. N., Washizu, R., Yasuda, T., & Minobe, S. (2017). Sea level variability around Japan during the twentieth century simulated by a regional ocean model. *J. Clim.*, *30*(14), 5585–5595. doi: 10.1175/JCLI-D-16-0497.1

Slangen, A. B., Meyssignac, B., Agosta, C., Champollion, N., Church, J. A., Fettweis, X., ... others (2017). Evaluating model simulations of twentieth-century sea level rise. part i: Global mean sea level change. *J. Clim.*, *30*(21), 8539–8563. doi: 10.1175/JCLI-D-17-0110.1

Storelvmo, T., Heede, U. K., Leirvik, T., Phillips, P. C., Arndt, P., & Wild, M. (2018). Lethargic response to aerosol emissions in current climate models. *Geophys. Res. Lett.*, *45*(18), 9814–9823. doi: 10.1029/2018GL078298

Suzuki, T., & Ishii, M. (2011). Long-term regional sea level changes due to variations in water mass density during the period 1981–2007. *Geophys. Res. Lett.*, *38*(21). doi: 10.1029/2011GL049326

Suzuki, T., & Ishii, M. (2015). Interdecadal baroclinic sea level changes in the North Pacific based on historical ocean hydrographic observations. *J. Clim.*, *28*(11), 4585–4594. doi: 10.1175/JCLI-D-13-00103.1

Suzuki, T., & Tatebe, H. (2020). Future dynamic sea level change in the western subtropical north pacific associated with ocean heat uptake and heat redistribution by ocean circulation under global warming. *Prog. Earth Planet. Sci.*, *7*(1), 1–10. doi: 10.1186/s40645-020-00381-9

Terada, M., & Minobe, S. (2018). Projected sea level rise, gyre circulation and water

mass formation in the western north pacific: Cmip5 inter-model analysis. *Clim. dyn.*, *50*(11), 4767–4782. doi: 10.1007/s00382-017-3902-8

Tsujino, H., Nakano, H., & Motoi, T. (2008). Mechanism of currents through the straits of the japan sea: Mean state and seasonal variation. *J. Oceanogr.*, *64*(1), 141–161. doi: 10.1007/s10872-008-0011-7

Urakawa, L. S., Tsujino, H., Nakano, H., Sakamoto, K., Yamanaka, G., & Toyoda, T. (2020). The sensitivity of a depth-coordinate model to diapycnal mixing induced by practical implementations of the isopycnal tracer diffusion scheme. *Ocean Modell.*, *154*, 101693. doi: 10.1016/j.ocemod.2020.101693

Wild, M. (2016). Decadal changes in radiative fluxes at land and ocean surfaces and their relevance for global warming. *Wiley Interdiscip. Rev.: Climate Change*, *7*(1), 91–107. doi: 10.1002/wcc.372

Wild, M., Ohmura, A., & Makowski, K. (2007). Impact of global dimming and brightening on global warming. *Geophys. Res. Lett.*, *34*(4), 1–4. doi: 10.1029/2006GL028031

Yasuda, T., & Sakurai, K. (2006). Interdecadal variability of the sea surface height around Japan. *Geophys. Res. Lett.*, *33*(1), 2–5. doi: 10.1029/2005GL024920

Yukimoto, S., Kawai, H., Koshiro, T., Oshima, N., Yoshida, K., Urakawa, S., ... Ishii, M. (2019). The meteorological research institute Earth system model version 2.0, MRI-ESM2.0: Description and basic evaluation of the physical component. *J. Meteorol. Soc. Jpn.*, *97*(5), 931–965. doi: 10.2151/jmsj.2019-051

Zhang, L., & Delworth, T. L. (2015). Analysis of the characteristics and mechanisms of the pacific decadal oscillation in a suite of coupled models from the geophysical fluid dynamics laboratory. *J. Clim.*, *28*(19), 7678–7701. doi: 10.1175/JCLI-D-14-00647.1

Zhong, Y., & Liu, Z. (2009). On the mechanism of pacific multidecadal climate variability in ccsm3: The role of the subpolar north pacific ocean. *J. Phys. Oceanogr.*, *39*(9), 2052–2076. doi: 10.1175/2009JPO4097.1

Figure1.

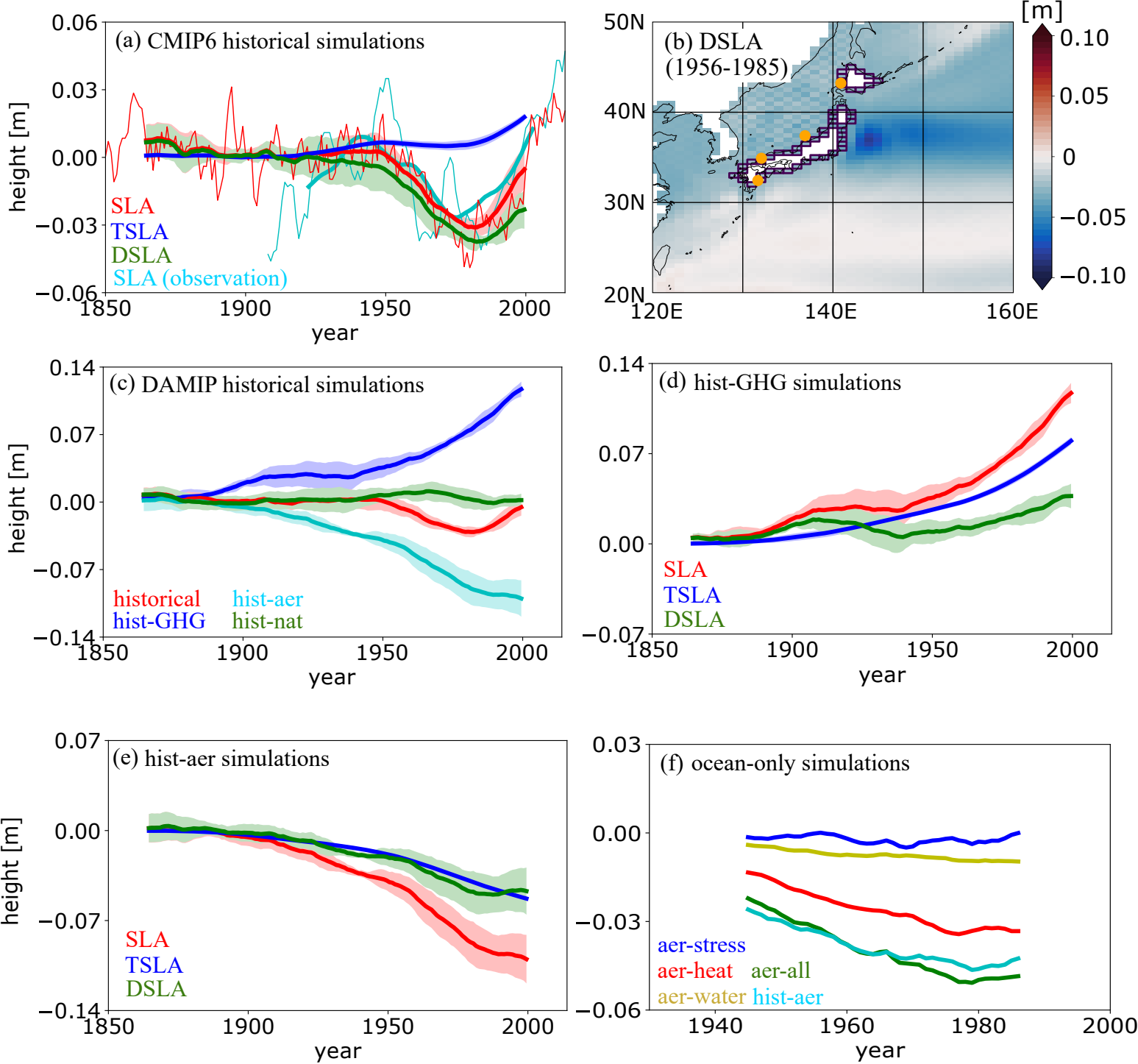
(a) CMIP6 historical simulations
height [m]
year
SLA
TSLA
DSLA
SLA (observation)
(b) DSLA
(1956-1985)
[m]
(c) DAMIP historical simulations
historical
hist-GHG
hist-aer
hist-nat
(d) hist-GHG simulations
(e) hist-aer simulations
(f) ocean-only simulations
aer-stress
aer-heat
aer-water
aer-all
hist-aer

Figure2.

60N
45N
30N
15N
(a) surface heat flux
−12 −6 0 6 12
[W m^{-2}]

(b) SWR
−12 −6 0 6 12
[W m^{-2}]

(c) LWR
−12 −6 0 6 12
[W m^{-2}]

(d) turbulent heat flux
−12 −6 0 6 12
[W m^{-2}]

(e) AOD
−0.2 −0.1 0 0.1 0.2

(f) SWR (All Sky-Clear Sky)
−12 −6 0 6 12
[W m^{-2}]

(g) SST
−1.6 −0.8 0 0.8 1.6
[℃]

(h) SLP
−100 −50 0 50 100
[Pa]

(i) DSL (1.5 layer model)
120E 180 120W
−0.1 −0.05 0 0.05 0.1
[m]

(j) DSL
120E 180 120W
−0.06 −0.03 0 0.03 0.06
[m]

Figure3.

60N
45N
30N
15N
120E
180
120W
(a) fafstress
(b) fafheat
(c) fafall
(d) linear
−0.06
−0.03
0
0.03
0.06
[m]
Depth [m]
0
500
1000
1500
20
25
30
35
40
45
50
(e) fafstress
(f) fafheat
(g) fafall
(h) linear
18
12
6
(i) fafstress
(j) fafheat
(k) fafall
(l) linear
−1.2
−0.6
0.6
1.2
[℃]

Supporting Information for "Effects of Anthropogenic Forcings on Multidecadal Variability of the Sea Level around the Japanese Coast Simulated by MRI-ESM2.0 for CMIP6"

Yusuke Ushijima[1,2], Hiroyuki Tsujino[2], Kei Sakamoto[2], Masayoshi Ishii[2],

Tsuyoshi Koshiro[2], Naga Oshima[2]

[1]Japan Meteorological Business Support Center, Tsukuba, Japan

[2]Meteorological Research Institute, Tsukuba, Japan

Contents of this file

Text S1. Flux calculation for sensitivity experiments

Here, the method of the flux calculation in ocean-only sensitivity experiments are described in detail. The fluxes in the ocean model were calculated as described in Urakawa et al. (2020) although surface atmospheric variables for the flux calculation were 3-hourly piControl atmospheric data in our simulations unlike Urakawa et al. (2020) where those from an atmospheric reanalysis are used. For sensitivity experiments except control simulation, flux perturbations are added to the fluxes calculated in the model as in the Flux-Anomaly-Forced Model Intercomparison Project (FAFMIP) (Gregory et al., 2016). The flux perturbations in this study are the monthly mean anomalies of one member of the hist-aer simulations (whose initial condition is taken from piControl output in 1850) relative to the piControl simulation as shown in Fig. S1 although the figure shows the flux anomalies averaged in 1956–1985. Unlike FAFMIP, temporal variations of the flux perturbations longer than interannual time scale are considered in these sensitivity experiments. The anomalies of surface wind stress, heat flux, and freshwater flux are imposed in ocean-only-aer-stress, ocean-only-aer-heat, and ocean-only-aer-water simulations, respectively, while all fluxes are simultaneously applied in ocean-only-aer-all simulation. Note that imposed heat flux anomaly changes the sea surface temperature (SST) and modifies the heat flux to oppose the anomaly as indicated Gregory et al. (2016). To avoid this negative feedback, the method B of Gregory et al. (2016) was applied. In the method B, a passive tracer T_R, initialized to initial temperature in the ocean, is introduced. It is changed by model's surface heat flux heat flux without anomaly and transported as the same way to the temperature in the ocean model that feels the heat flux anomaly. For

the flux calculation in the model, T_R at the surface is used as the SST instead of the SST calculated in the model. Thus, the SST for the flux calculation, or T_R at surface, is not directly affected by the heat flux anomaly.

Due to these flux anomalies, the dynamic sea level (DSL) changes. Figure S2 shows the DSL changes due to the flux anomalies. The change in the ocean-only-aer-water simulation is much smaller than the others in the western North Pacific, thus the surface freshwater flux change has a minor impact on DSL change in the western North Pacific in comparison to the other flux changes.

References

Gregory, J. M., Bouttes, N., Griffies, S. M., Haak, H., Hurlin, W. J., Jungclaus, J., ... Winton, M. (2016). The Flux-Anomaly-Forced Model Intercomparison Project (FAFMIP) contribution to CMIP6: Investigation of sea-level and ocean climate change in response to CO2 forcing. *Geosci. Model Dev.*, *9*(11), 3993–4017. doi: 10.5194/gmd-9-3993-2016

Urakawa, L. S., Tsujino, H., Nakano, H., Sakamoto, K., Yamanaka, G., & Toyoda, T. (2020). The sensitivity of a depth-coordinate model to diapycnal mixing induced by practical implementations of the isopycnal tracer diffusion scheme. *Ocean Modell.*, *154*, 101693. doi: 10.1016/j.ocemod.2020.101693

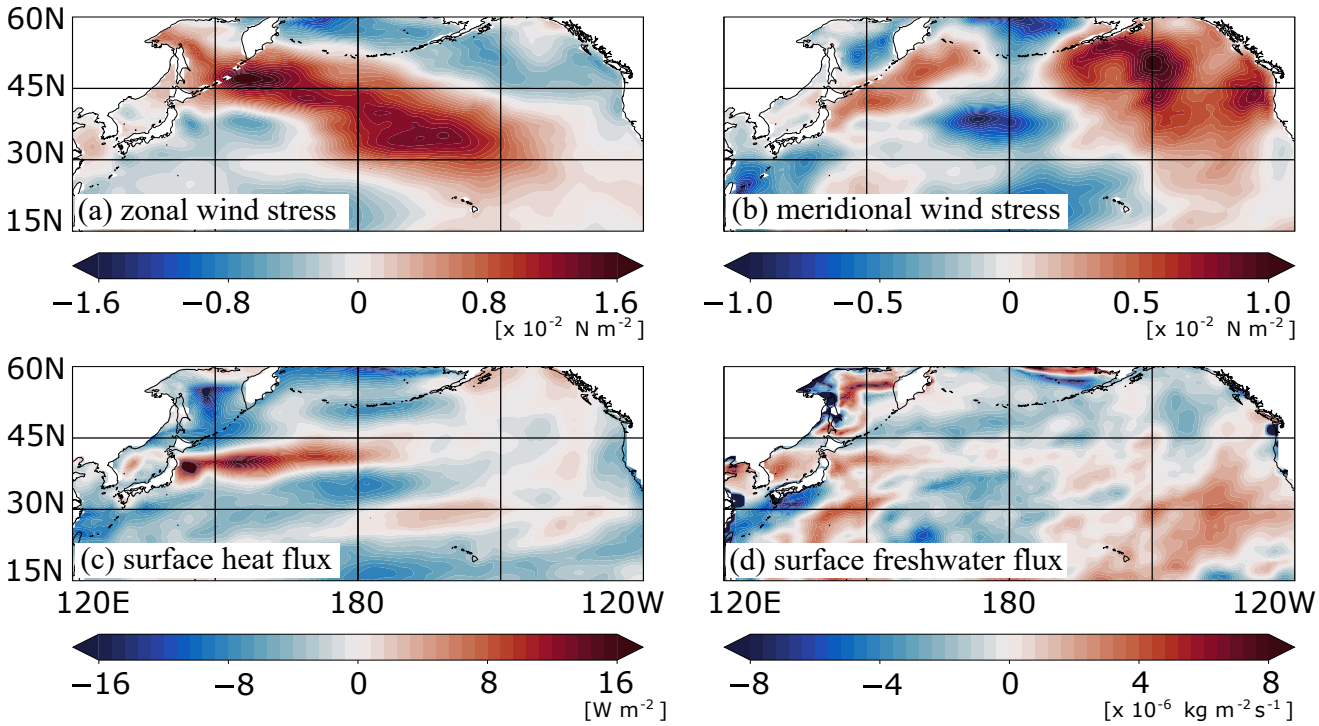

Figure S1. The anomalies of the surface (a) zonal wind stress, (b) meridional wind stress, (c) heat flux, and (d) freshwater flux in the North Pacific in the member of the hist-aer simulations relative to the piControl simulation averaged in 1956–1985.

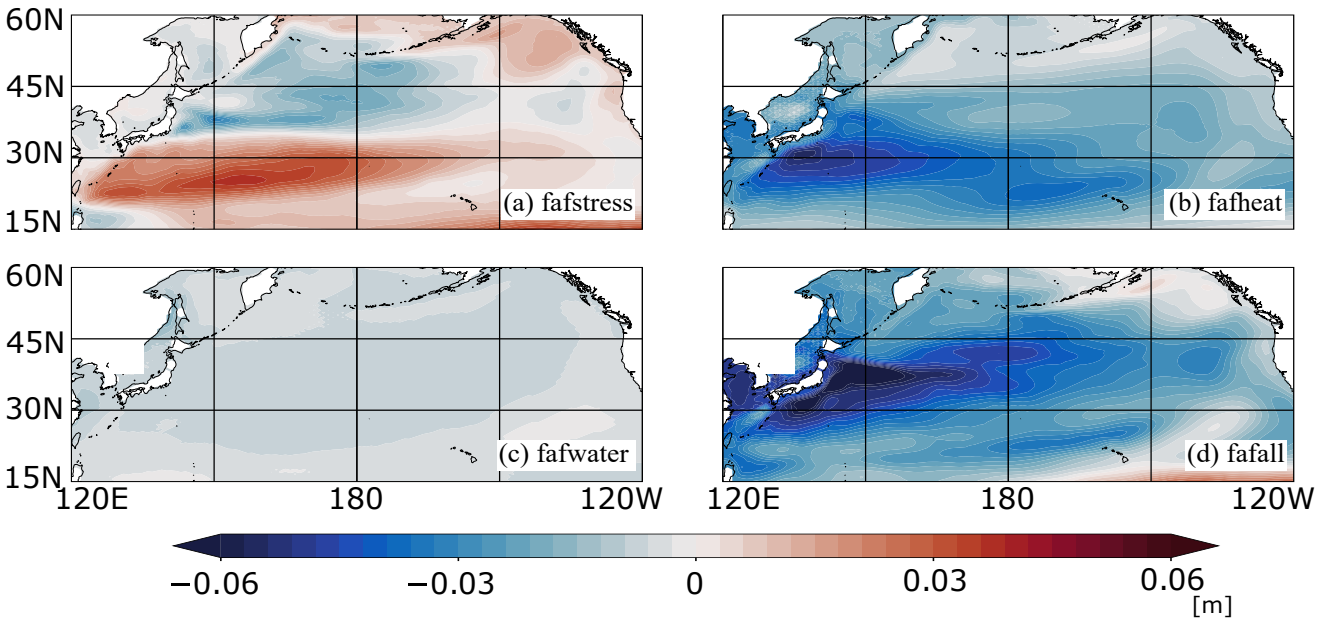

Figure S2. The DSLA in the North Pacific in the (a) ocean-only-aer-stress, (b) ocean-only-aer-heat, (c) ocean-only-aer-water, and (d) ocean-only-aer-all simulations. All variables are averaged in 1956–1985. The panels of (a), (b), and (d) are same as those in Figs. 3a-c.

Table S1. List of experiments by MRI-ESM2.0

Name of experiment	ensemble member
historical	5
hist-GHG	5
hist-aer	5
hist-nat	5
piControl	1

Table S2. List of sensitivity experiments by MRI-COM4

Name of experiment	added surface flux anomaly (hist-aer - piControl)
ocean-only-aer-stress	Wind stress anomaly
ocean-only-aer-heat	Surface heat flux anomaly
ocean-only-aer-water	Surface water flux anomaly
ocean-only-aer-all	Wind stress, surface heat flux, and surface water flux anomalies
ocean-only-control	-